Universitat de Barcelona &

Universitat Autonoma de Barcelona

UNIVERSITAT DE BARCELONA

UAB

Universitat Autònoma de Barcelona

Ultra-High Resolution seismic imaging in the Gulf of Cadiz for natural hazard assessment

Reservoir Geology and Geophysics

Master's Thesis

by

Ennio Piazza

Advisor: Beatriz Benjumea and

Rafael Bartolomè

ABSTRACT

2D Ultra-High Resolution multichannel seismic reflection profiles, collected during INSIGHT project survey cruises over the period between the 29th April and 17th may 2018, have enabled characterising the subsurface structural elements of the Marques de Pombal fault, Lineation South East, and Ginsburg Mud Volcano in the Gulf of Cádiz, from about 600m to 1600 m water depth. The aim of the INSIGHT project is to determine the seismic hazard in the area from the study of the active faults in relationship with the presence of active fluid seepage. The geology and the morphology of the surveyed areas are very variable.

The aim of this work is to process 2D UHR data in order to provide the best quality and resolution in the seismic imaging. In this work, three of the forty four acquired profiles will be presented. The first one is on the active fault of Marques de Pombal in front of Lisbon coast, the second one on a strike-slip fault 300km long in the south area of the Gulf of Cadiz, and the third is on top of two mud volcanos, about in the same area of the second profile. The data were acquired in different areas with different geological and geomorphological setting: it was necessary to differentiate the processing flow in each areas in order to preserve the primary signal and avoid multiple, diffractions, artefact and any kind of noise.

The data show compressive structures, strike-slip fault, extensional faults, salt tectonic features and in general a very complex geology, with a very high resolution and quality. The processing flow is performed to enhance the primary signal and to eliminate the artefacts, multiples and noise. This propose was successfully achieved

1. INTRODUCTION

The 2D UHR (Ultra High Resolution) seismic “INSIGHT” survey was conducted in the area of Gulf of Cadiz to investigate, with the highest possible resolution, the active structures (faults and landslides), within the Portuguese and Moroccan waters. The Gulf of Cadiz concentrates the largest events in West Europe. The survey is focus specially in the large seismogenic structures, such as the Marques de Pombal Fault and Lineament South (part West), which accommodate part of the African-European plate convergence. These faults may be the sources of large destructive events, such as the historical 1755 Lisbon earthquake (Mw 8.5) or the 1969 Horseshoe Earthquake (Mw 8.0) (Gracia et al., 2016). (Figure1.1)

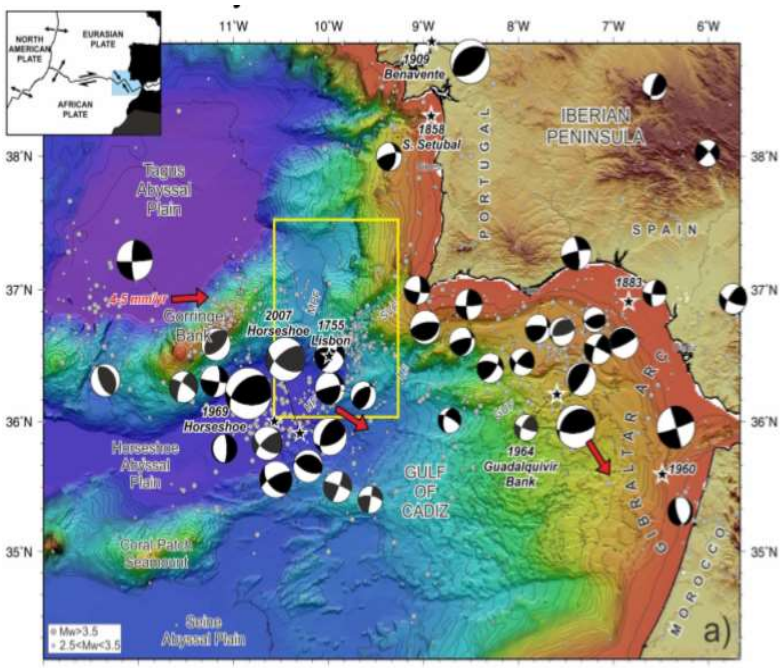

Figure 1.1 Active Sismicity and focl mechanism in the Gulf of Cadiz (Gracia et al., 2016) in the yellow rectangle the areas of study

To determine the seismic hazard in a fault is necessary to assess the rate at which a fault slips because average earthquake recurrence intervals tend to decrease as slip rates increase. For this reason, it is critical to understand the physical phenomena and definition of the fault seismic parameters regarding the Fault geometry (e.g. length, dip, max. seismogenic depth, segmentation). 2D high resolution seismic is critical to accurately obtain dip- and strike-slip rates and to image the fault seismic parameters. The goal of this work is to produce an interpretable dataset of the 2D HR seismic profiles, in migrated time sections and RMS velocities, to further measure and calculate the fault seismic parameters. These last two points are out of the scope of this work because it will imply a large amount of interpretation time using all dataset recorded and published in the study area.

The acquired data was quality checked and processed on-board of the survey vessel and in the laboratory latter on, using RadexPro seismic processing software. Each stage of quality control (which involved examining raw data gathers, a near trace gather and stacks of the seismic data) and processing (which involved vary denoise, demultiple and migration routines) was checked and tested in order to set up the best general parameters and particular as well adapted to each profile.

One of the most human time consuming processing steps consists on velocity picking along the seismic sections. Velocity picks for all lines were also checked using velocity-time maps and NMO corrected CDP gathers. Stacks were produced after each stage of the processing flow to test each parameter, specially carefully controlling the quality of the seismic images to ensure the integrity of the data by avoiding removing primary data.

2. GEOLOGICAL SETTING

Bordering the Mediterranean, the Gulf of Cádiz has experienced a northwest-southeast convergence from the LateMiocene to the Present (Maldonado et al., 1999; Nocquet and Calais 2004). Westward movement and collision of the Alborán Domain with the southern Iberian and North African margins gave rise to the development of a wedge of chaotic internal character in the Gulf during the late Tortonian (Fig.1.1), reaching the Horseshoe abyssal plain (Maldonado et al., 1999; Somoza et al., 1999; Medialdea et al., 2004). It has been interpreted as an accretionary prism related to an east-dipping subduction zone beneath Gibraltar, which is either currently active or not according to different authors (Maldonado et al., 1999; Gutscher et al., 2002; Zitellini et al., 2009). In Figure 1.1, the wedge is neatly delineated on the bathymetric map along the broad continental slope, where two arcuate-shaped lobes together with their deformation fronts are also visible (Gutschern et al., 2009).

In the SW Iberian Margin, seismicity is characterized by shallow to deep earthquakes of low to the moderate magnitude (Mw < 5.5) (Buforn et al., 1995, 2004, Stich et al., 2005, 2007, 2010). However, this region is also the source of the largest and most destructive earthquakes that have affected Western Europe (AD 1531, 1722, 1755 and 1969) (Fukao 1973) (Figure.1.1). The 1755 Lisbon Earthquake (estimated Mw > 8.5) destroyed Lisbon (intensity X-XI MSK). The event was accompanied by one tsunami that devastated the SW Iberian and NW African coasts (Baptista et al., 1998, Baptista and Miranda 2009). None of the tsunami models satisfactorily accounts for the estimated magnitude of the earthquake and tsunami arrival times at the different localities onshore. The deployment of 24 OBS (Ocean Bottom Seismographs) during a year at the external part of the Gulf of Cadiz, shows that earthquakes in the Horseshoe Abyssal Plain are generated in the upper mantle at depths between 40 and 60 km (Stich et al., 2010, Geissler et al., 2010). Along the same line the Horseshoe Abyssal Thrust (HAT), has been identified on wide-angle seismic modeling as the source of deep earthquakes (Martínez-Loriente et al., 2014).

In the INSIGHT project, a total of 44 MCS profiles were acquired between -10.3°W and -6.9°W and 34.9° and 37°N following mainly NE-SW and W-E directions (Appendix Table 9.1). The survey has been conducted in the SW Iberian margin encompassing a very large area. In this work, the results of three lines will be presented acquired in 3 different areas (Figure 2.1):

-the Marques de Pombal thrust fault (line MP08b)

-the main tectonic strike-slip structures and salt diapirism structures in the Lineation South East (line LSE06)

-the Ginsburg Mud Volcano (line GMV01).

The exact coordinates of Start of Line and End of all the lines are reported in the Appendix Table 9.1

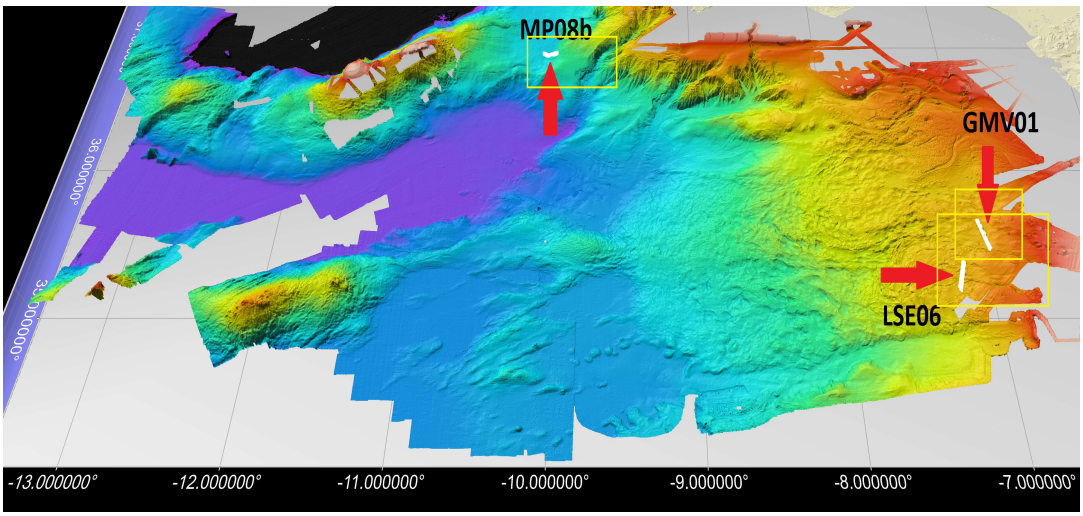

Figure 2.1: MultiBeam data of Gulf of Cadiz area with the surveyed lines highlighted. In yellow rectangles the areas of study for the Insight project.

3. 2D UHR ADQUISITION PARAMETERS: Source, Receivers, Offsets and Recording Settings

Between April 29th and May 17th 2018, the INSIGHT survey was focused on the acquisition of Multichannel Seismic Reflection (MCS) data using the digital, solid state, 443.75m long streamer and the source airgun system of the Unidad de Tecnología Marina (UTM – CSIC, Spain) onboard R/V Sarmiento de Gamboa. A total 44 MCS profiles were acquired, three of them will be presented in this work.

Source. In the table 3.1 the source parameters are presented. In the Figure 3.1 the deploying setting of the gun cluster is shown

Table 3.1 Guns Specifications.

SOURCE PARAMETERS	
Source controller	Big Shot®
Source type	G-GUN II®
Air pressure	2000 psi
Volume	930 cu.in / 650 cu.in
Total number of guns	10-8
Gun synchronization	+/- 0.1 ms
Deployment depth	3.6 m (3.5 theoretical)
Shot interval	12,5/ 18.5 / 25 m (depending on the area)

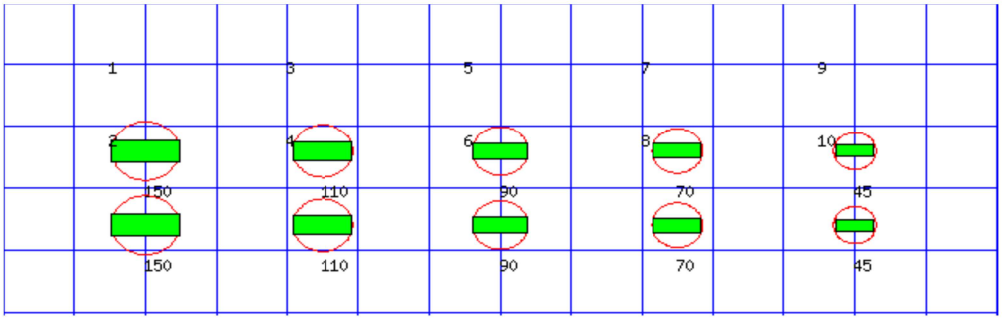

Figure 3,1 guns array: numbers above red circles are the volume in cu,in of the correspondent gun. The longitudinal distance between the guns: 2.5m

Receivers. The specification of the streamer are reported in the table 3.2.

Table 3.2 General acquisition parameters of the streamer used during INSIGHT seismic profiles

STREAMER PARAMETERS	
Streamer model	GeoEel®
No. of hydrophones per channel	8
Depth	3.5 m
Active channels	72
Active length	443.75 m
Group interval	6.25 m
No. birds (all of them with compasses)	3
CMP distance	3.125 m
Auxiliary channels	4

Offset. The offset between source, receiver and GPS position is reported in the Figure 3.2

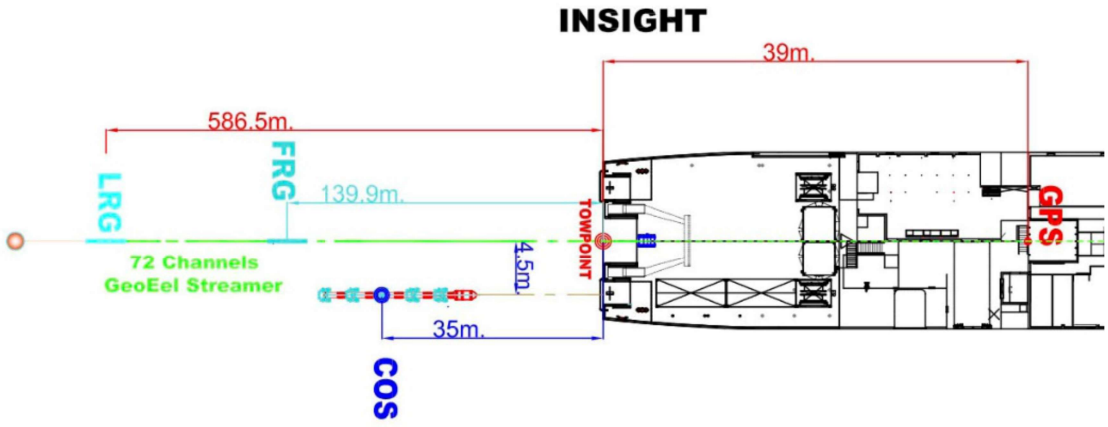

Figure 3.2 General offset for seismic acquisition system used during INSIGHT survey on Samiento de Gamboa R/V

Recording settings. Record length and sample interval are set up to best fit with the water depth, the maximum possible penetration and the main frequencies of the source. In the deep water areas (about 3000-4000m) the record length was 8000ms

and in the shallow areas was 6000ms. The sample interval is 1ms, which corresponds to a Nyquist of 500Hz.

4. METHODS: processing flow

As mentioned in this work three of the forty four acquired line are presented and the processing flow applied to the line GMV01 is discussed. In general, the processing flow is quite similar for all sites but, as any of them are located in very different geological environment with particular geophysical, geological and geomorphological characteristics, the processing flow was adapted for each site in order to obtain the best results. All the rest of the setting parameters applied to each processing step was tested to get the best result, it means that they can largely vary from site to site. For instance, profiles acquired in very deep water, the surface related multiple is not recorded or, at least, does not affect the primary signal arrivals. Consequently the demultiple routines has not been applied in deep waters.

The processing flow of the line GVM01 is the most complex and exhaustive in this work and for this reason it was chosen to be presented in this work. Nevertheless, many other routine was tested without satisfactory results and are not included in the manuscript. The processing flow was performed with the RadexPro seismic software utility. The main processing steps are:

Reformatting

Raw field data in SEG-D format were reformatted into RadexPro internal processing format. An Ormsby BandPass filter (5-10-400-500 Hz) was applied in order to remove low frequency noise (normally due to the swell noise) and avoid aliasing effect. The data was resampled to 1ms (Nyqyst frequency 500Hz: according to the source characteristics) and shifted 50ms upwards to compensate the time delay applied by the acquisition system. A second static shift is applied to compensate the streamer and source tow depth (3.5m+3.5m= 7m = 5ms). (Figure 4.1)

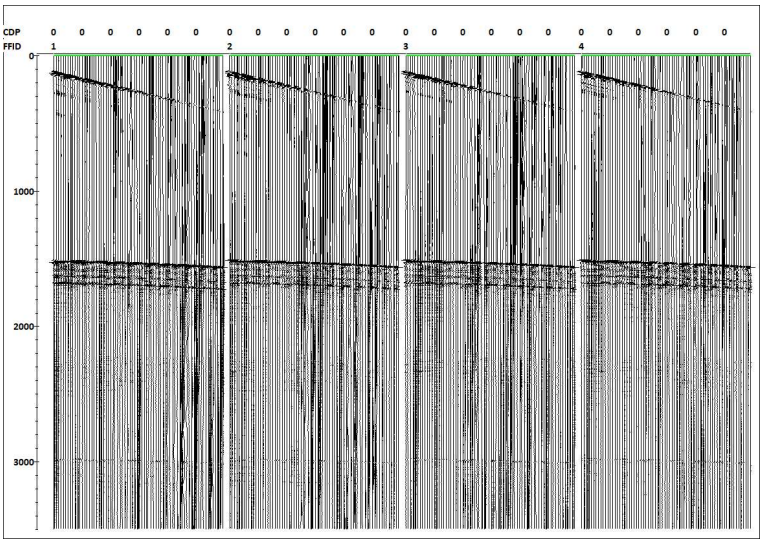

a

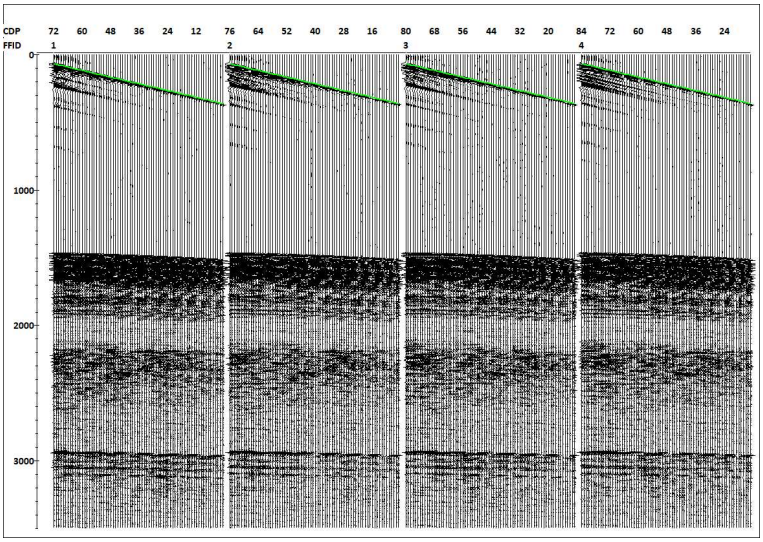

b)

Figure 4.1 Shot Gather: a) raw data; b) Static delay, Band Pass Filter and Resample applied, Vertical scale of Two Way Travel Time (TWTT) in milliseconds (ms)

Geometry assigned

Real geometry was calculated and added to trace headers, using the positioning file from navigation system and the offset diagram provided by the acquisition team.

Qc Steps and Water Bottom Picking

Near trace gathers were used to interactively pick a direct arrival time and water bottom (seafloor) time for use in later processing. Data were immediately controlled on-board of the survey vessel, in order to identify items that may have an adverse effect on data quality, e.g. wrong calculated direct offset, bad channels or noisy records. The seabed was then top-muted.

DeBubble

The “bubble effect” (the effect due to the secondary collapses and expansions of the compressed air bubble) is present and evident in all the data. This effect reduce the resolution of the data. To remove it the following procedure was applied:

All the traces were selected and stacked in order to create a unique wavelet where the primary signal and the bubble are enhanced while on the contrary the signal due to the geology is reduced. The operator for the deconvolution is output from this stacked trace. In the next step this operator is use to deconvolve all the traces. The routine can be applied in any gather, in this case it was applied in the receiver gather.(Figure 4.2)

a)

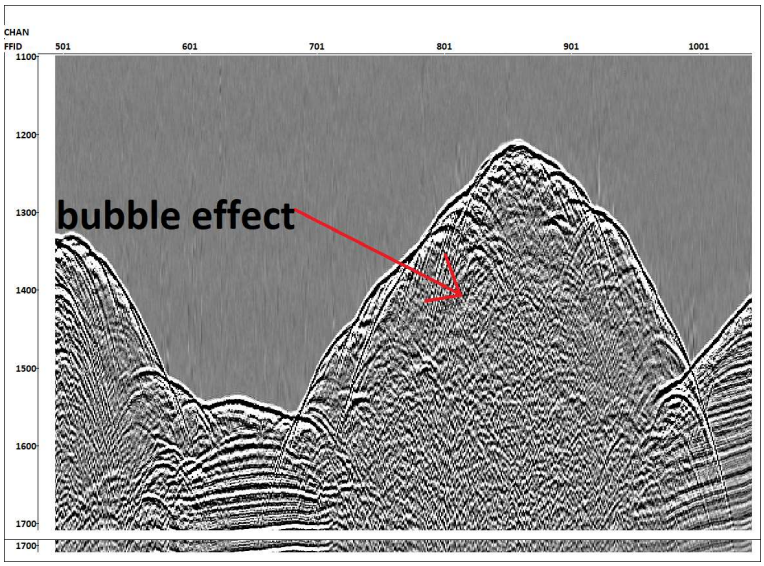

b)

Figure 4.2 Receiver Gather: a) Static delay, Band Pass Filter and Resample applied; b) Debubble applied to previous image. Vertical scale of TWTT in ms

Sharp Seis Deghosting

SharpSeis Deghosting routine is dedicated for removing ghost wavefield from marine seismic data. The ghost effct is due to the reflection of the primary signal in the interface of air and water. This effect depends from the depth of the receiver and the source and from the frequency of the signal. The SharpSeis Deghosting module utilize a stabilized approximate recursive filter solution, applied to a seismic trace in both forward and reversed time. The resulting two traces (primary wavefield without the ghost, and ghost wavefield without the primary) are, then, combined in a nonlinear manner in order to maximize the signal and suppress the noise trains, stabilizing the result even further. The optimum ghost delay is estimated adaptively to the data within a sliding window, to ensure the best possible match. This results in sharp crystal-clear seismic images with high signal-to-noise ratio.

This routine is applied in the receiver gathers. As the streamer and the source where at about 3,7m, the parameters of the deghosting routine were chosen to best fit with this acquisition setting. As sown in the Figure 4.3, it enhances the energy of the primary wavelet and reduce the length of it.

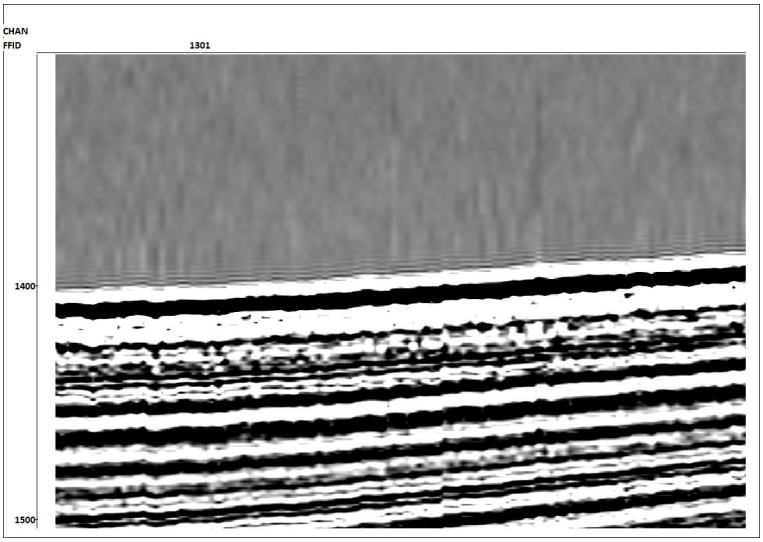

a)

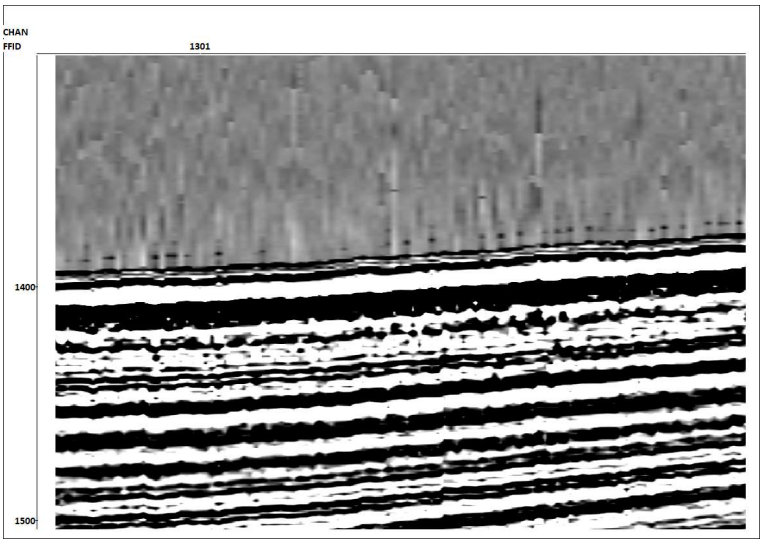

b)

Figure 4.3 Receiver gather: a) Static delay, Band Pass Filter, Resample and Debubble applied; b) Deghosting applied to previous image. Vertical scale of TWTT in ms

Time Frequency Domain NoiseAttenuation (TFDN)

The module is designed for attenuation of noises localized in frequency domain and possibly in time domain as well. It allows to remove local narrow frequency band noises without affecting the spectrum of the remaining record.

For each trace of a seismogram in the indicated time window the amplitude spectrum is computed. The time window width identifies the amount of frequency samples that the amplitude spectrum is subdivided into (the smaller the window width, the less the frequency samples aj mount (the bigger the frequency sampling interval).

For the whole seismogram (or specified ensemble of traces), the median value is computed for each frequency sample.

The median value of the received medians multiplied by the specified multiplier is taken as a threshold value for the whole seismogram.

Every frequency sample is compared with the indicated threshold value. If the value in the current sample exceeds the threshold one, it is replaced with the average value computed on

the basis of the traces set indicated in the Trace Aperture parameter and within the same frequency band.

The multiplier parameter (Threshold Multiplier) allows a user to control the threshold value as it makes it possible to avoid too «strong» (with too low value) or insufficient (with too high threshold value) amplitude balancing.

In this case the routine is applied in the CDP gather with NMO applied (with rought velocity profile) in order to best preserve the primary signal and remove the random ambient noise and the possible artifacts created in the previous deghosting routine. The NMI is than apllied to come back to the original data aspect. The effect of this routine is not appreciable at the scale and resolution of this paper, for this reason the results are not shown in this work.

Zero Phase Deconvolution

A zero phase conversion filter was derived from an extracted seafloor reflection wavelet. To generate the wavelet, the same procedure of the debubble routine was use. All the trace of the data were stacked to create a single representative wavelet. The onset of the negative kick on the seafloor was set to time zero. The extracted wavelet is used to deconvolve the dataset. (Figure 4.4)

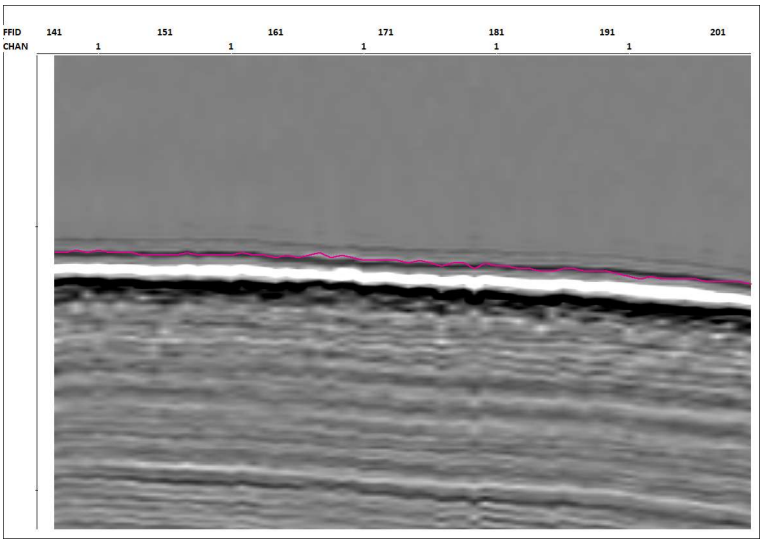

a)

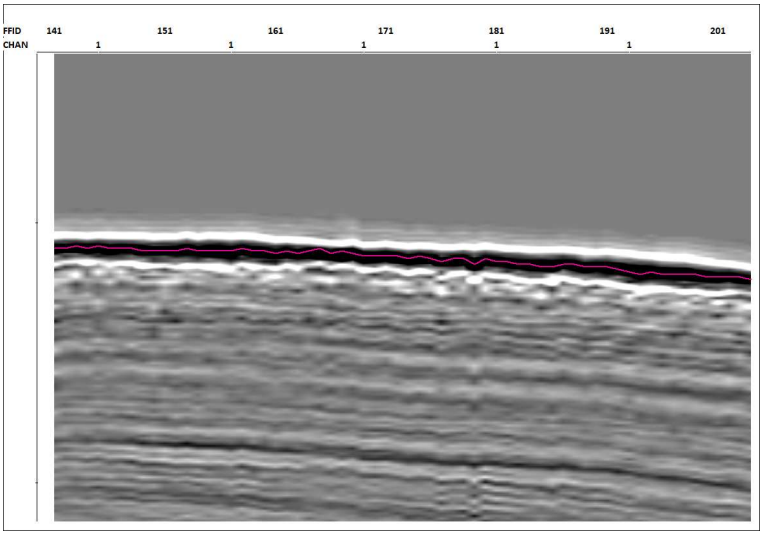

b)

Figure 4.4 Receiver gather: a) Static delay, Band Pass Filter, Resample and Debubble applied; b) Zero Phase deconvolution applied to previous image. Vertical scale of TWTT in ms

Velocity Picking

A high resolution velocity analysis using Normal Move Out (NMO) correction was conducted for each line using the Interactive Velocity Analysis software (IVA RadexPro internal software). The analysis was performed at 500m intervals, with each location being compared to and constrained by neighbouring locations. This ensured that consistency was maintained between adjacent lines and velocity locations. (Figure 4.5)

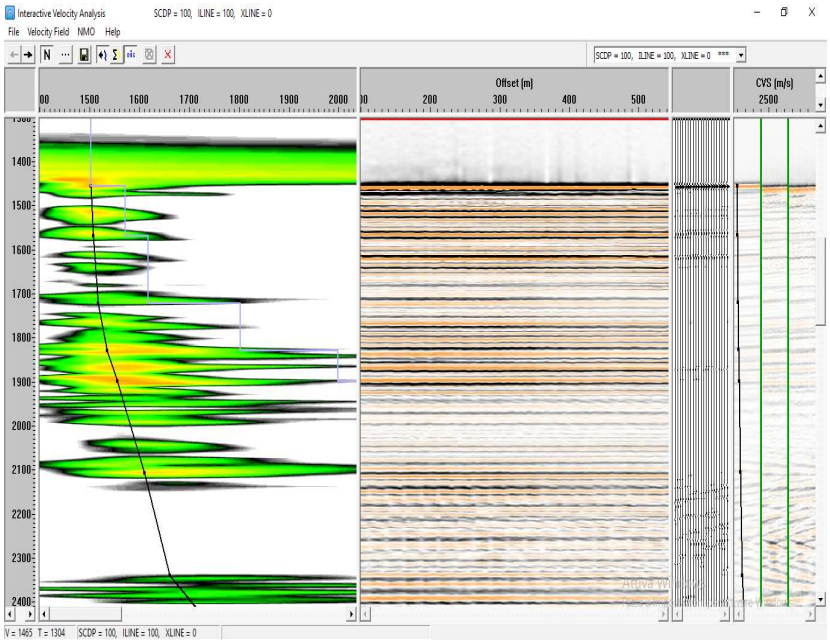

a) *b)* *c)* *d)*

Figure 4.5 Interactive Velocity Analysis a) calculated semblance; b) Supergather with NMO applied with the picked velocity; c) portion of stack with picked velocity applied; d) portions of stack with different velocity picking

Navigation Merge

The trace and CDP positions are calculated merging the navigation file provided by the navigation system. Dummy shots were added where needed in order to compensate possible miss shots.

CDP sorting. NMO and stack

The data is sorted by CDP gather. NMO is applied with picked velocities. Testing of multiple mutes for stack response was carried out to achieve the optimal result. Mean algorithm is used for trace normalization when stacking.(Figure 4.6)

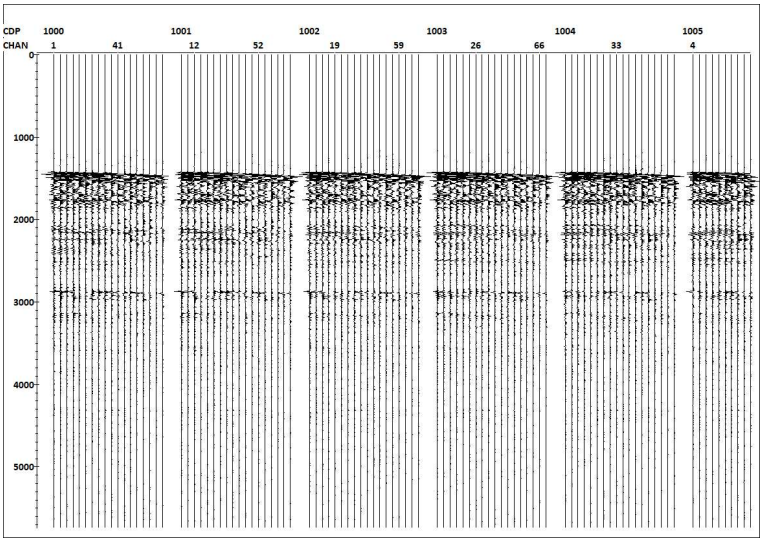

a)

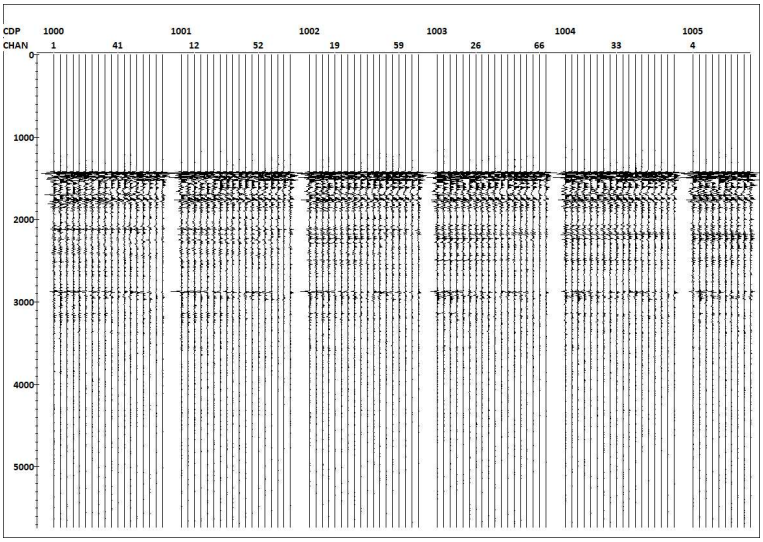

b)

Figure 4.6 Receiver gather: a) Static delay, Band Pass Filter, Resample, Debubble and Zero Phase deconvolution applied; b) NMO applied to previous image. Vertical scale of TWTT in ms

Spherical Divergence Correction

A gain recovery proportional to RMS velocities was applied to the data to account for geometric spreading loss of energy.(Figure 4.7)

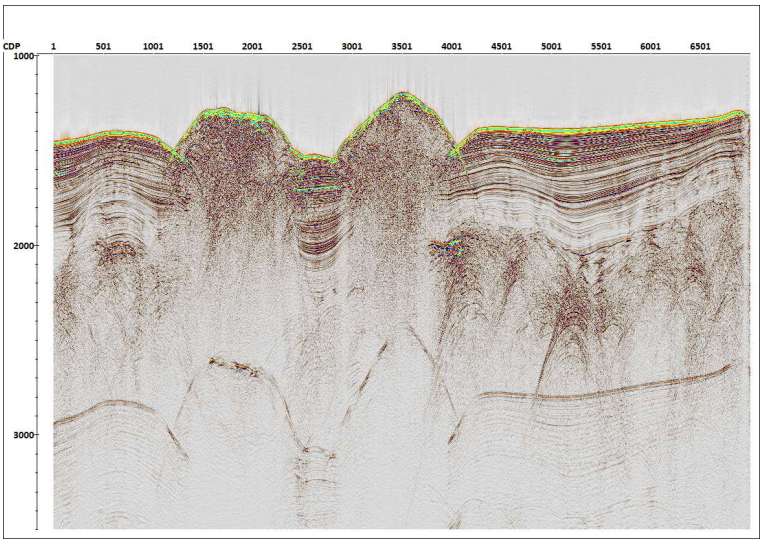

a)

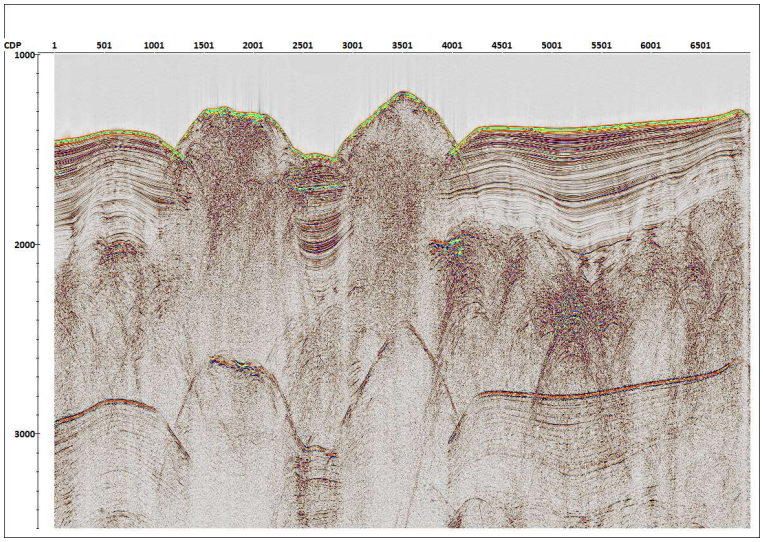

b)

Figure 4.7 Stack: a) Stack from Static delay, Band Pass Filter, Resample, Debubble, Zero Phase deconvolution and NMO applied: b) Stack with Spherical Divergence

Zero-offset Demultiple

The module is deigned for demultiple of near-offset single-channel or stacked seismic data. In this case the module is used in the stack. The algorithm is based on adaptive subtraction of a model of multiples from the original wave field. The model is obtained from the data itself, either by static shift of the original traces of by autoconvolution.(Figure 4.8)

In general terms, a special filter is calculated for each trace basing on both the original data traces and the model traces. This filter, when applied to the trace is trying to minimize the RMS amplitudes of whatever is found similar between the trace and the model. The more similar is the model of multiples to the real multiples observed, the more efficient is the subtraction. For this reason the most accurate multiple modeling can be easily made on zero-offset or stacked data.

In this case, to remove the multiple is very difficult. The water bottom in fact is affected by many diffraction. The multiple energy of the diffraction is not very consistent. For this reason

the multiple model in this area does not fit with the real multiple energy present in the data, and consequently the adaptive subtraction does not work perfectly. This routine was applied three times to get a better result. The consequence is that the multiple is not completely removed. Many other demultiple routine (SRME, FK, Radon, Deconvolution) were taken and, in case, tested. None of them gave good results as this routine did.

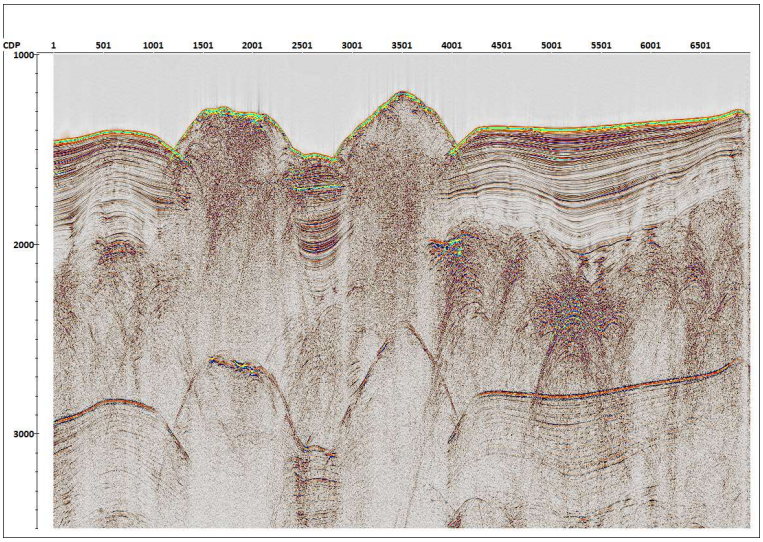

a)

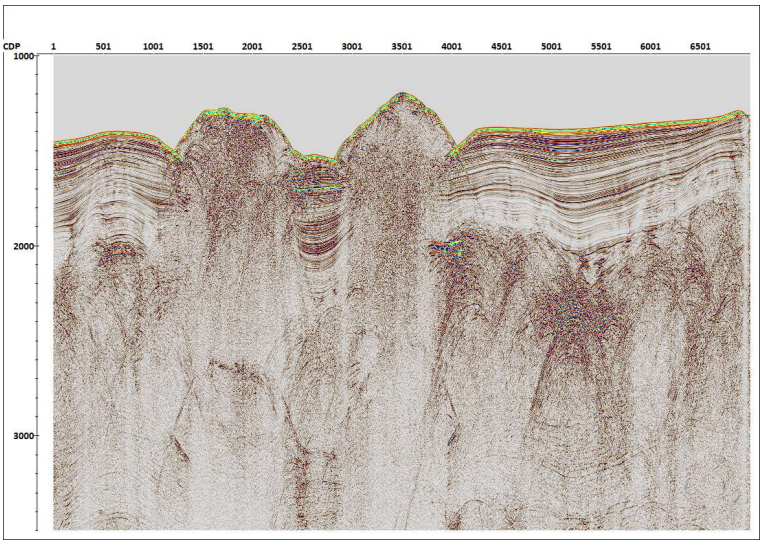

a the migration point at specific times in meters. It is variable and increasing with time. The aperture profile is customized to best collapse the diffractions.

The signal can be starched when migrated. The stretching factor depends on the time and position of the input trace relative to the output trace. Stretching usually becomes smaller as the time increases, and becomes larger as the angle between the output sample and the CDP increases. Migration stretching is a phenomenon common to all types of migration. The Stretch muting allows avoiding this problem. Proper values are tested and applied. All frequencies above 80% Nyquyst frequency of the input data (80% of 500Hz= 400Hz) will be filtered out. The traces will be resampled to an interval at which the specified frequency will become the new Nyquist frequency. This technique speeds up the migration procedure

significantly. After completion of data migration, the original sampling interval is restored. (Figure 4.9)

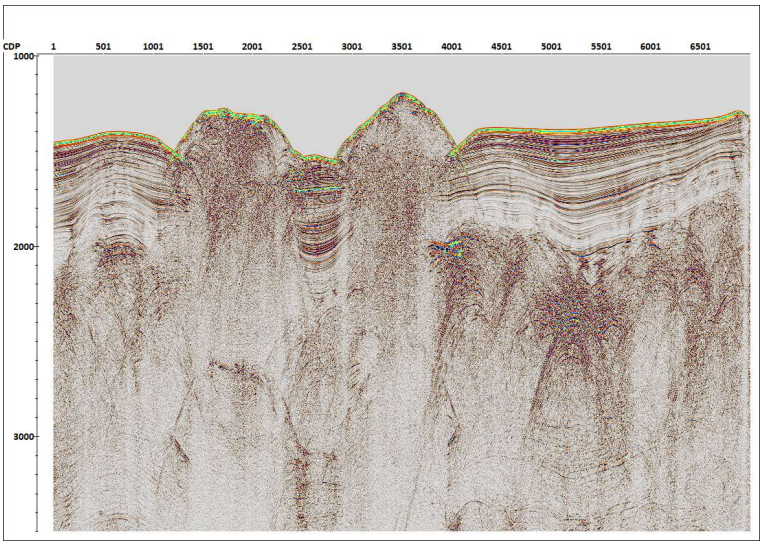

a)

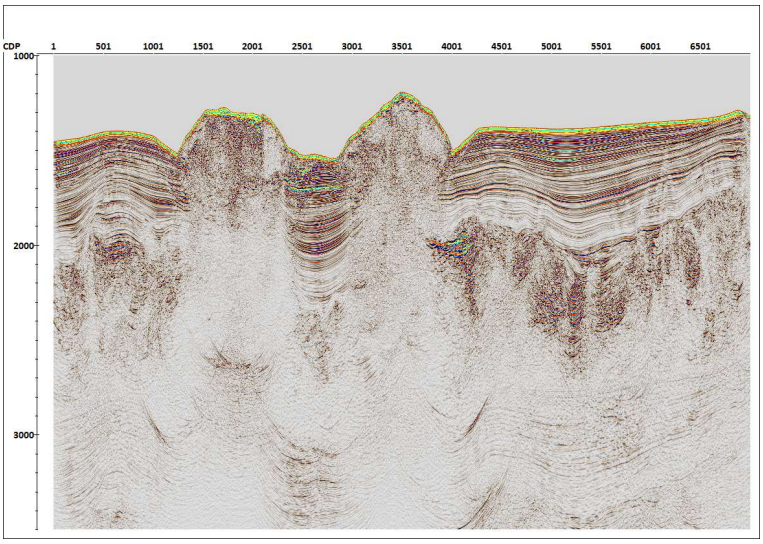

b)

Figure 4.9 Stack: a) Stack with Spherical Divergence and zero-offset Demultiple; b) Kirchhoff Mgration applied to the previous image

Time Variant Scaling

A time variant scaling is applied to recovery the loss amplitude due to the migration routine. (Figure 4.10)

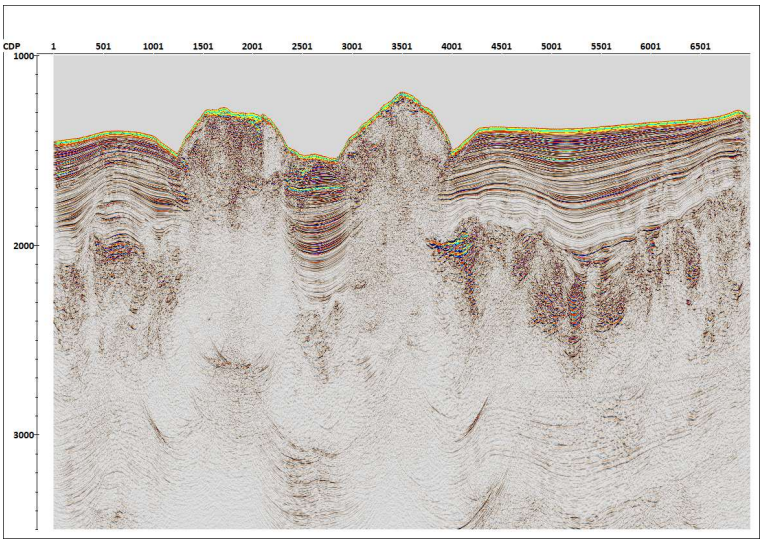

a)

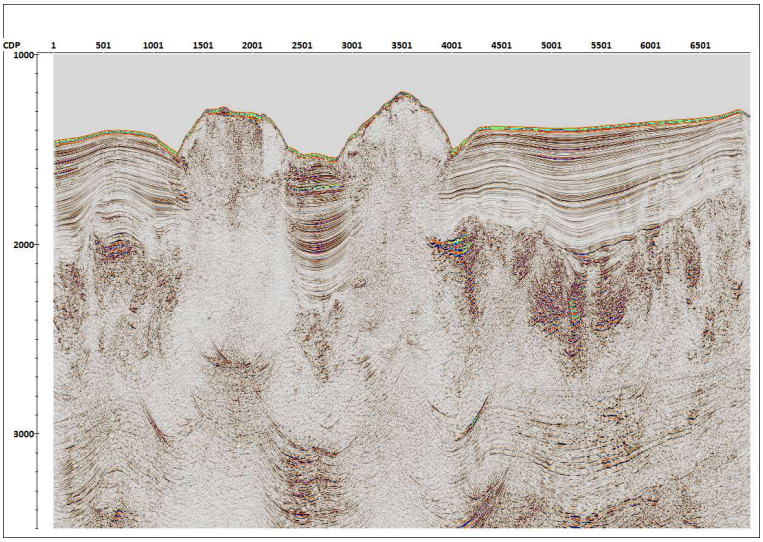

b)

Figure 4.10 Stack: a) Stack with Spherical Divergence, zero-offset Demultiple and Kirchhoff Mgration; b) Time Variant Scaling applied to the previous image

5. RESULTS

Three profiles from three different sites are shown in the following figures. The lines are MP08b (Figures 5.1a and 5.1b), LSE06 (Figures 5.2a and 5,2b), GMV01 (Figures 5.3a and 5,3b). For each line brute stack and fully processed stack are shown.

a)

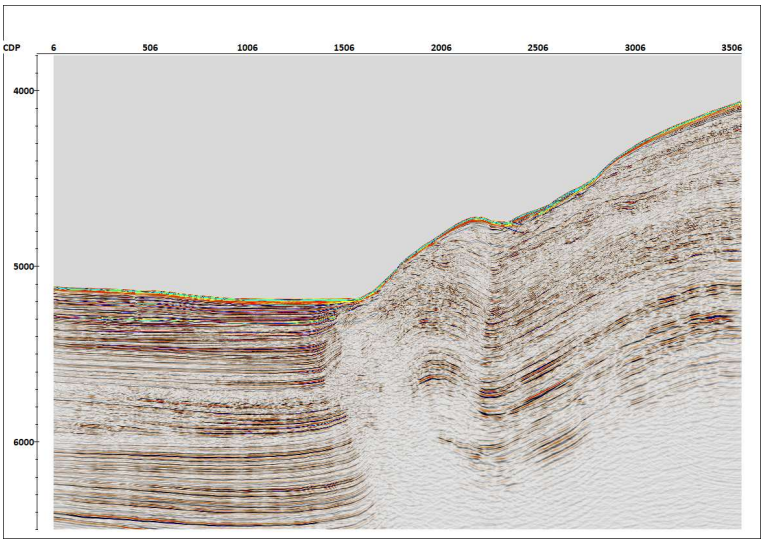

b)

Figure 5.2 stacks: a) LSE06 Brute Stack; b) LSE06 Fully Processed Stack

a)

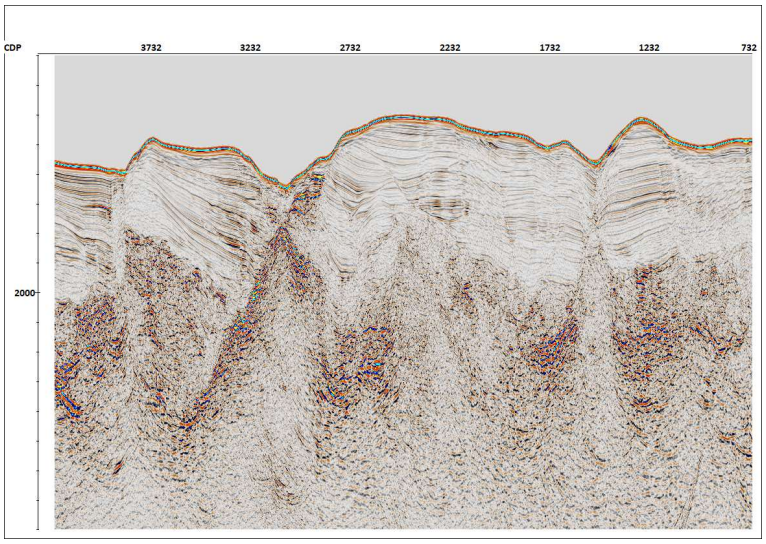

b)

Figure 5.2 stacks: a) LSE06 Brute Stack; b) LSE06 Fully Processed Stack

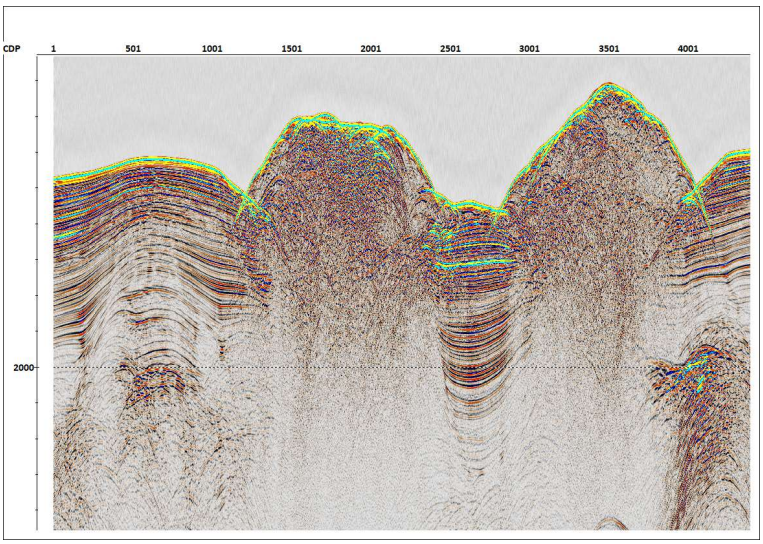

a)

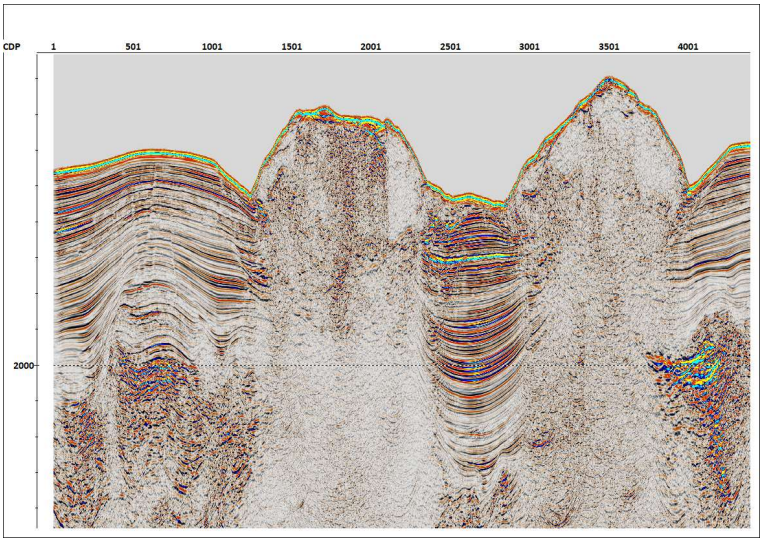

b)

Figure 5.3 stacks: a) GMV01 Brute Stack; b)GMV01 Fully Processed Stack

6. DISCUSSION

Determine the presence of active fluid seepage and characterize its relationship with the occurrence of geohazard-related features

The occurrence of earthquakes and submarine landslides is strongly dependent on the build-up of pore pressure in the deep and shallow subsurface respectively. Occurrence of pockmarks, mud volcanoes and salt diapirs at the seafloor evidence fluid flow systems and presence of overpressures at various depths. In the Gulf of Cadiz abundant salt and shale diapirism exists it has been shown that there is a close relationship between mud volcanoes, diapirs and tectonic structures (Toyos et al., 2016) . However, the relationship between fluid seepage, faulting and submarine landsliding is not well constrained in the external Gulf of Cadiz. We could characterize in detail the occurrence of these focused fluid flow systems and determine their relationship to active faulting. We could use this profile to determine whether

the origin of the fluids is deep or relatively shallow, which might result in significantly different types of geohazards (earthquakes vs. landslides). We can also investigate if fluids seep at locations where earthquakes nucleate at depth and try to reveal active venting of fluids in the water column analysing the first tens of meters of the seismic profile. In the Figure 6.1 the image from Toyos et al., 2016 and in Figure 6.2 the image from the processing performed for this work

Figure 7.1.Ginsburg Mud Volcano from Toyos et al., 2016

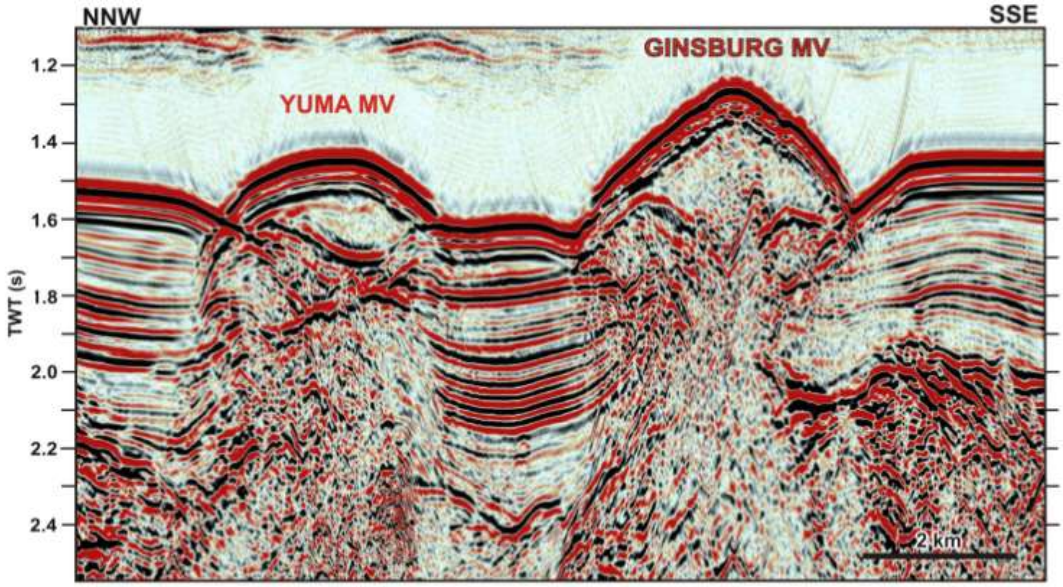

Figure 7.2 Ginsburg Mud Volcano processed for this work

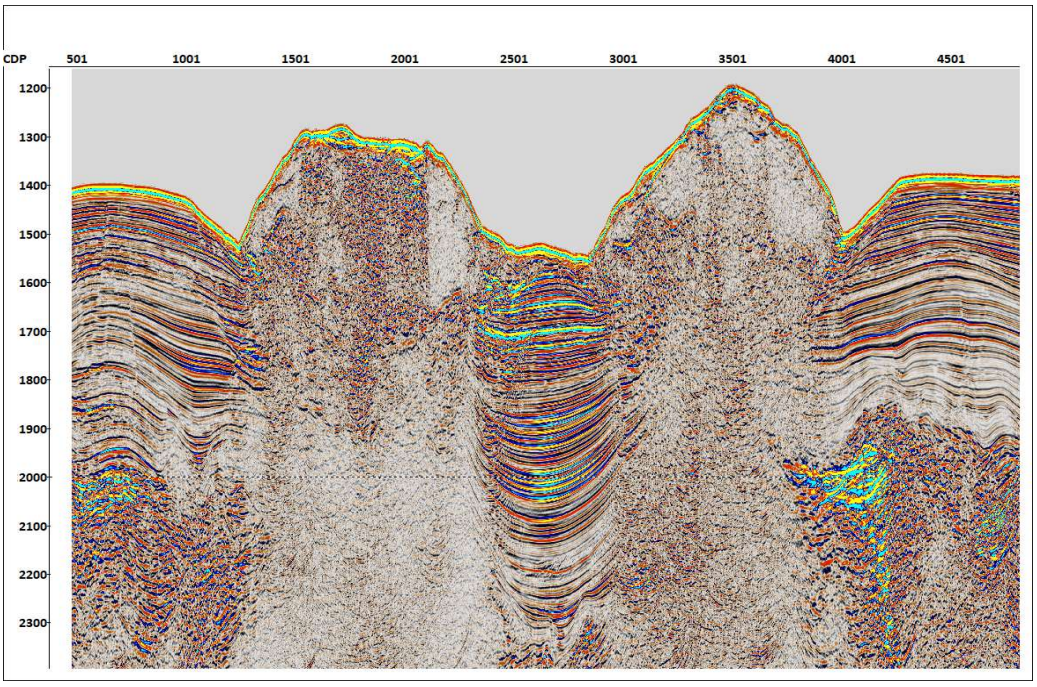

7. CONCLUSIONS

Regarding the quality of the results and the interpretation of the seismic profiles, the propose of the work was successfully achieved: the seismic lines were processed providing a high quality imaging, suitable for the geological risk assessment. In particular it is possible to better observe the relationship with the active fluids and faults.

Regarding the processing, the resolution of the data was enhanced and level of noise reduced. In some lines, the multiple energy wasn't completely removed, but it doesn't drastically affect the data, because the residual multiple energy doesn't obliterate the primary signal. As the morphology of the seabed and the geological feature are often very complex, one of the most critical step of the processing is the Kirchhoff Migration: many and very variable diffractions were present and, consequently it was quite difficult to choose the correct aperture parameters. A variable aperture was applied, different from site to site.

7.ACKNOWLEDGEMENTS

I have to thanks three groups of people:
The first one is made by all the people involved in the INSIGHT project: scientists, technicians and crew. They made the life on board of the Sarmiento de Gamboa very pleasant, in particular I have to thanks Eulàlia Gràcia and Roger Urgeles to have given to me the opportunity to be involved in this very interesting project.
The second one is the group of my college in the master, very good friends helping me a lot during this long year.
The third one is the most important: my family, supporting me in every moment.

8. REFERENCES

Baptista, M. A., Heitor, S., Miranda, J., Miranda, P., & Mendes Victor, L. (1998). The 1755 Lisbon tsunami; evaluation of the tsunami parameters. J. Geodyn. 25: 143–157.

Baptista, M. A. & Miranda, J. M. (2009). Revision of the Portuguese catalog of tsunamis. Nat Hazards Earth Syst Sci 9: 25–42.

Bartolome, R., Gràcia, E., Stich, D., Martínez-Loriente, S., Klaeschen, D., Mancilla, F. L., Lo Iacono, Cl., Dañobeitia, J.J., & Zitellini N. (2012). Evidence for active strike-slip faulting along the Eurasia-Africa convergence zone: Implications for seismic hazard in the southwest Iberian margin. Geology 40: 495–498.

Buforn E, Sanz de Galdeano C & Udıas A. (1995). Seismotectonics of the Ibero-Maghrebian region. Tectonophysics 248: 247– 261.

Buforn, E., Bezzeghoud, M., Udías, A. & Pro, C. (2004). Seismic Sources on the Iberia-African Plate Boundary and their Tectonic Implications. Pure Appl. Geophys. 161: 623–646.

Fukao, Y. (1973). Thrust faulting at a lithospheric plate boundary the Portugal earthquake of 1969. Earth. Planet. Sci. Lett. 18: 205–216.

Geissler, W. H., Matias, L., Stich, D., . Carrilho, F., Jokat, S. Monna, W., Iben Brahim, A.., Mancilla, F., Gutscher, M.-A., Sallarès V. & Zitellini, N. (2010). Focal mechanisms for sub-crustal earthquakes in the Gulf of Cadiz from dense OBS deployment. Geophys. Res. Lett. 37: L18309.

Gutscher MA, Malod J, Rehault JP, Contrucci I, Klingelhoefer F, Mendes-Victor L, & Spakman W (2002) Evidence for active subduction beneath Gibraltar. Geol Soc Am 30(12): 1071–1074.

Gutscher MA, Dominguez S, Westbrook GK, Gente P, Babonneau N, Mulder T, Gonthier E, Bartolome R, Luis J, Rosas F, Terrinha P, The Delila, DelSis Scientific Teams (2009) Tectonic shortening andgravitational spreading nin the Gulf of Cadiz accretionary wedge:observations from multibeam bathymetry and seismic profiling.Mar Pet Geol 26: 647–659.

Maldonado A, Somoza L, & Pallarés L (1999). The Betic orogen and the Iberian-African boundary in the Gulf of Cádiz: geological evolution (Central North Atlantic) deployment. Mar Geol 155: 9-43.

Medialdea T, Vegas R, Somoza L, Vázquez JT, Maldonado A, Díaz delRío V, Maestro A, Córdoba D, & Fernández-Puga MC (2004) Structure and evolution of the Olistostrome complex of the Gibraltar Arc in the Gulf of Cádiz (eastern Central Atlantic): evidence from two long seismic cross sections. Mar Geol 209: 173–198.

Nocquet JM, & Calais E (2004) Geodetic measurements of crustal deformation in the western Mediterranean and Europe. Pure ApplGeophys 161: 661–681.

Somoza L, Maestro A, & Lowrie A (1999) Allochthonous blocks as hydrocarbon traps in the Gulf of Cadiz. Proc Offshore Technol Conf10889: 571–577.

Stich D., Mancilla F.L. & Morales J.(2005). Crust-mantle coupling in the Gulf of Cadiz (SW-Iberia). Geophys. Res. Lett. 32: L13306.

Stich D., Mancilla F, Pondrelli S, & J. Morales J (2007). Source analysis of the February 12th, 2007, Mw 6.0 Horseshoe earthquake: Implications for the 1755 Lisbon earthquake. Geophys. Res. Lett. 34: L12308

Stich D., Martín, R. & Morales, J. (2010). Moment tensor inversion for Iberia–Maghreb earthquakes 2005–2008. Tectonophysics 483: 390–398.

Toyos M, Medialdea T , León R, Somoza L, González FJ, & Meléndez N (2007). Evidence of episodic long-lived eruptions in the Yuma, Ginsburg Jesús Baraza and Tasyo mud volcanoes, Gulf of Cádiz Geo-Mar Lett (2016) 36: 197–214.

Zitellini N, Gràcia E, Matias L, Terrinha P, Abreu MA, De Alteriis G, Henriet JP, Dañobeitia JJ, Masson DG, Mulder T, Ramella R, Somoza L, & Diez S (2009) The quest for the Africa-Eurasia plate boundary west of the Strait of Gibraltar. Earth Planet Sci Lett 280: 13–50.

9. APPENDIX

Table 9.1 Start of Line and End of Line of all the acquired lines

AREA	LINE	SOL (Lat)	SOL (Lon)	EOL (Lat)	EOL (Lon)
Marques de Pombal Fault	TMP03b	036°52'18.81491"	-009°51'55.81063"	036°55'31.81571"	-010°00'7.93055"
	MP03b	036°55'46.47209"	-010°00'50.46996" 875555557777777 77	036°58'4.58344"	-010°07'37.71447"
	MP04b	036°56'49.74831"	-010°07'48.05036"	036°54'23.85766"	-010°00'44.98421"
	MP05b	036°53'23.25764"	-010°01'35.90648"	036°55'48.99879"	-010°08'43.13334"
	MP06b	036°54'35.44436"	-010°08'59.96047"	036°52'7.31878"	-010°01'48.83405"
	MP07b	036°51'12.74374"	-010°03'2.06302"	036°53'36.52385"	-010°09'58.02698"
	MP08b	036°52'14.90075"	-010°09'52.71748"	036°49'56.42087"	-010°03'9.05378"
	MP09b	036°48'55.49423"	-010°04'0.65492"	036°51'19.62669"	-010°11'1.48633"
	MP11b	036°49'44.79903"	-010°08'52.86043"	036°51'1.51559"	-010°08'17.71963"
	MP11c	036°51'27.79608"	-010°08'11.66303"	036°58'37.01937"	-010°06'39.07305"
Lineation South Western	TLSW01	035°44'38.34111"	-010°02'29.03931"	035°46'42.19772"	-010°05'36.21445"
	LSW01	035°46'21.64088"	-010°07'34.96034"	035°37'4.39849"	-010°10'11.93185"
	LSW02	035°37'56.37562"	-010°13'52.48388"	035°47'22.14483"	-010°11'12.73520"
	LSW08	035°39'1.44027"	-010°05'49.04692"	035°45'20.71032"	-010°03'49.80627"

	LSW09	035°44'50.73464"	-010°02'12.99033"	035°38'28.19348"	-010°04'12.24603"
	LSW10	035°38'23.14691"	-010°02'43.92729"	035°44'47.84894"	-010°00'44.20283"
	LSW11	035°44'13.32480"	-009°59'25.04220"	035°37'47.15460"	-010°01'25.10100"
	LSW12	035°43'56.18657"	-009°58'1.78289"	035°37'34.33183"	-010°00'1.87863"
Part	LSW13	035°37'28.14631"	-009°58'18.01884"	035°43'46.31017"	-009°56'19.93299"
	LSW14	035°43'16.09286"	-009°54'55.40551"	035°36'51.48692"	-009°56'57.40282"
	LSW15	035°36'56.90754"	-009°55'36.52516"	035°43'22.00708"	-009°53'35.39039"
	LSW16	035°42'46.09368"	-009°52'25.87969"	035°36'23.78930"	-009°54'24.86602"
AREA	**LINE**	**SOL (Lat)**	**SOL (Lon)**	**EOL (Lat)**	**EOL (Lon)**
	LSW17	035°42'27.66180"	-009°50'57.09120"	035°36'9.08040"	-009°53'1.07880"
Lin-eation South Western Part	LSW18	035°33'42.08760"	-009°50'40.29600"	035°43'6.77640"	-009°47'39.06840"
	LSW19	035°42'16.00860"	-009°44'39.19320"	035°32'52.56120"	-009°47'33.77400"
	LSW20	035°32'40.00800"	-009°44'14.98080"	035°41'58.46760"	-009°41'16.91520"
	LSW23	035°46'5.53800"	-010°12'57.02800"	035°39'24.152400"	-009°40'30.22000"
	LSE03	035°11'40.89780"	-007°20'46.52040"	035°01'49.55160"	-007°24'13.69140"
	LSE05	035°01'23.95380"	-007°20'51.06240"	035°11'8.78700"	-007°17'26.25120"
Lin-eation South Eastern Part	LSE06	035°11'38.29320"	-007°15'22.45560"	035°00'49.43340"	-007°19'10.29420"
	LSE07	035°00'40.47480"	-007°17'39.26340"	035°10'47.82300"	-007°14'6.91980"
	LSE08	035°09'53.35920"	-007°12'53.23980"	035°00'9.23760"	-007°16'18.84900"
	LSE09	034°59'55.21080"	-007°14'11.10420"	035°09'34.98900"	-007°10'46.32720"
	LSE13	035°08'30.73260"	-007°06'50.83500"	035°00'13.71900"	-007°09'46.14360"
	LSE15	035°00'40.43880"	-007°08'48.73680"	035°04'15.74220"	-007°24'39.13800"
Gins-burg Mud Vul-cano	GMV1	035°28'6.18960"	-007°06'27.21540"	035°16'30.67260"	-007°03'48.51720"
	GMV2	035°16'43.13340"	-007°03'49.45500"	035°16'41.54817"	-007°03'47.24837"
	GMV3	035°21'26.65200"	-007°12'4.19820"	035°21'25.81343"	-007°12'7.02045"
	PB1	036°05'44.31000"	-007°58'11.91240"	036°11'56.37120"	-008°04'16.27260"
	PB2	036°12'18.74940"	-007°58'16.99140"	036°05'25.97940"	-008°04'34.51680"
Por-timao Bank	PB3	036°03'48.30180"	-008°01'19.76340"	036°17'52.65600"	-007°59'17.47380"
	PB5	036°06'7.63440"	-008°04'42.35640"	036°07'27.37500"	-007°59'36.09420"
	PB6	036°09'44.40420"	-007°55'20.70480"	036°09'25.99740"	-008°07'21.27060"
	PB7	036°16'12.41700"	-008°00'47.69940"	036°19'23.86740"	-007°41'5.54880"